ELSEVIER

Materials Science and Engineering A 493 (2008) 123–129

MATERIALS SCIENCE & ENGINEERING A

www.elsevier.com/locate/msea

Determining the optimal stacking fault energy for achieving high ductility in ultrafine-grained Cu–Zn alloys

Y.H. Zhao [a], X.Z. Liao [b], Z. Horita [c], T.G. Langdon [d,e], Y.T. Zhu [a,*]

[a] *Material Physics and Application Division, Los Alamos National Laboratory, Los Alamos, NM 87545, USA*

[b] *School of Aerospace, Mechanical & Mechatronic Engineering, The University of Sydney, Sydney, NSW 2006, Australia*

[c] *Department of Materials Science & Engineering, Faculty of Engineering, Kyushu University, Fukuoka 819-0395, Japan*

[d] *Department of Aerospace & Mechanical Engineering and Materials Science, University of Southern California, Los Angeles, CA 90089-1453, USA*

[e] *Department of Materials Science, University of Southern California, Los Angeles, CA 90089-1453, USA*

Received 15 March 2007; received in revised form 15 November 2007; accepted 21 November 2007

Abstract

Bulk ultrafine-grained (UFG) materials produced by severe plastic deformation (SPD) often have low ductility. A previous study demonstrated the possibility of lowering the stacking fault energy to simultaneously increase the strength and ductility. This paper demonstrates, there exists an optimal stacking fault energy for the best ductility in UFG Cu–Zn alloys processed by the same SPD processing. When the stacking fault energy is too low, the grain size lies below 15 nm after SPD processing and the stacking faults are saturated so that it is difficult to accumulate dislocations and deformation twins during the subsequent tensile testing. These results provide significant guidance for the future design of UFG and nanocrystalline alloys for achieving high ductilities.

Keywords: Copper alloys; Ductility; High-pressure torsion; Severe plastic deformation; Stacking fault energy

1. Introduction

Ultrafine-grained (UFG) materials produced by severe plastic deformation (SPD) usually have high strength but disappointingly low ductility [1–7]. In practice, the low ductility of UFG materials severely limits their practical utility. Therefore, in recent years much attention has been devoted to developing strategies for improving the poor ductility of UFG materials [3,6–18]. The low ductility of UFG materials is attributed to the lack of strain hardening caused by their inability to accumulate dislocations because of their small grain sizes and saturation of dislocations [1,5,15–17]. By lowering the stacking fault energy of a copper alloy, it was reported recently that both dislocation accumulation and twin accumulation could be activated to improve the work hardening rate and consequently to increase the ductility while simultaneously improving the strength [16]. This raises a question: will the ductility continue to increase with decreasing stacking fault energy? Alternatively, is there an optimum stacking fault energy that yields the best ductility?

The objective of this study was to systematically investigate the effect of stacking fault energy on the ductility of ultrafine-grained/nanostructured Cu–Zn alloys. The investigation was conducted using Cu, a Cu–10 wt.% Zn alloy and a Cu–30 wt.% Zn alloy. The stacking fault energies of these materials are about 41 mJ/m^2, 22 mJ/m^2 and 7 mJ/m^2, respectively [19]. It is shown that the Cu–10 wt.% Zn exhibits the highest ductility, thereby suggesting there is an optimum stacking fault energy that yields the best ductility.

It is a special pleasure to present this paper within a symposium honoring Prof. Carl Koch. Over a long and

* Corresponding author. Now at: Department of Materials Science & Engineering, North Carolina State University, 1009 Capability Drive, Raleigh, NC 27695-7919, USA. Tel.: +1 9195130559; fax: +1 9195153419.
E-mail address: ytzhu@ncsu.edu (Y.T. Zhu).

0921-5093/$ – see front matter © 2007 Elsevier B.V. All rights reserved.
doi:10.1016/j.msea.2007.11.074

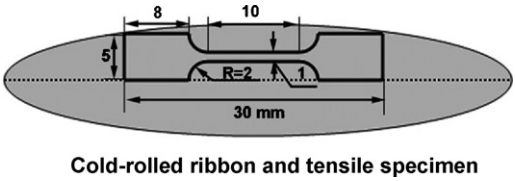

Fig. 1. Schematic representation showing cutting position of a tensile specimen from a UFG ribbon processed by HPT and cold rolling. The thickness of the tensile specimen was polished to 0.15 mm after cutting.

distinguished career, Carl has made many very significant contributions to our understanding of the processing, structures and properties of materials with nanocrystalline grain sizes.

2. Experimental materials and procedures

2.1. Sample preparation

Commercial copper (99.9%) and Cu–30 wt.% Zn alloy were purchased in the form of rods with a diameter of 10 mm and the Cu–10 wt.% Zn was purchased in the form of plates with a thickness of 6 mm. These materials were sliced into disks with thicknesses of 0.8 mm and diameters of 10 mm for processing by high-pressure torsion (HPT) [20,21]. The HPT was performed using a conventional facility in which the sample, in the form of a disk, is placed between a stationary upper and a rotational lower Bridgman anvil. Each disk was subjected to a total of five revolutions at room temperature using a rotation speed of 1 rpm with an imposed pressure of 6 GPa. The HPT-processed samples were then cold-rolled into thin ribbons with thicknesses of ~200 μm. The total thickness reduction for these samples was ~75% after multiple rolling passes with a thickness reduction of ~10% imposed in each pass.

2.2. Tensile testing

Tensile specimens were cut from the ribbons to have gauge lengths of 10 mm and widths of 1 mm as shown in Fig. 1 and they were then polished to a thickness of 0.15 mm. Uniaxial tensile tests were performed at room temperature using a Shimazu Universal Tester with an initial quasi-static strain rate of $1.7 \times 10^{-4}\ s^{-1}$. Five specimens were used for each condition to obtain consistent stress–strain curves.

Table 1
Lists of the yield strength ($\sigma_{0.2}$), uniform elongation (ε_u) (before necking) and elongation to failure (ε_e) of the HPT + cold-rolling processed Cu, Cu–10 wt.% Zn and Cu–30 wt.% Zn samples

	Samples		
	Cu (99.9%)	Cu–10 wt.% Zn	Cu–30 wt.% Zn
$\sigma_{0.2}$ (MPa)	420	580	690
ε_u (%)	2.2	3.8	3.2
ε_e (nm)	5.1	7.1	4.7

2.3. X-ray diffraction (XRD) measurements

Quantitative XRD measurements of the HPT + cold-rolling samples were performed on a Scintag X-ray diffractometer equipped with a Cu target operating at 1.8 kW and a graphite curved single-crystal ⟨0 0 0 2⟩ monochromator in order to select the Cu Kα radiation at the goniometer receiving slit section. The divergence and anti-scattering slits were chosen to be 0.5° and 0.5°, respectively, and the receiving slit had a width of 0.3 mm. The θ–2θ scans were performed to record the XRD patterns at room temperature. Pure Al powder (99.999%) was annealed at 200 °C in Ar and used as an XRD peak-broadening reference for the grain size and microstrain calculations. The peak parameters (peak intensity, peak-maximum position, full width at half maximum and integral breadth) were determined by fitting a Pearson VII function to the measured peaks. The XRD results were averaged from the whole ribbon samples and they represent the microstructural information along the cross-sectional direction of the HPT + cold-rolling samples.

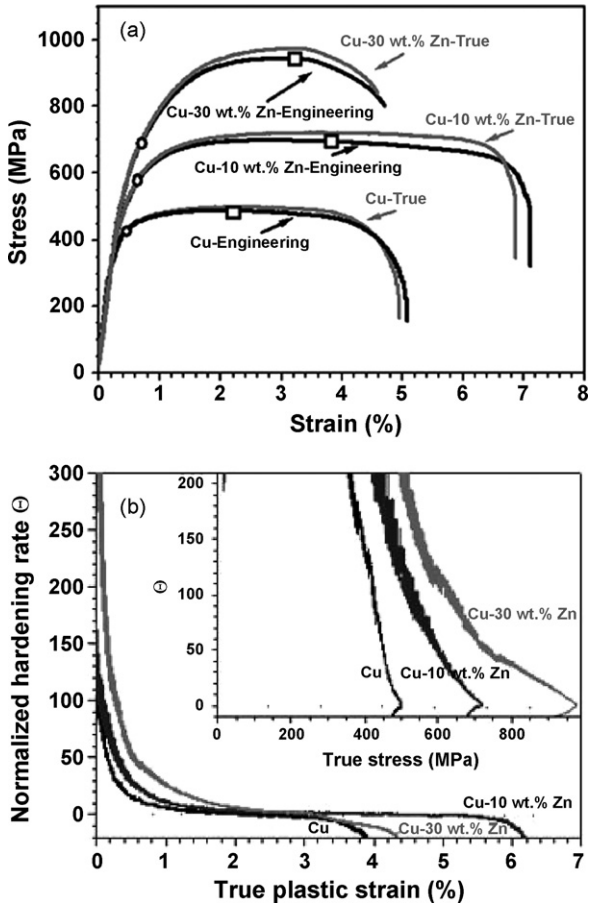

Fig. 2. (a) Tensile engineering and true stress–strain curves of the UFG Cu, Cu–10 wt.% Zn alloy, and Cu–30 wt.% Zn alloy. The open squares mark the uniform elongations and the open circles mark $\sigma_{0.2}$. (b) And the inset show the normalized work hardening rate, Θ, against the true stress. The true stress–strain curves and the Θ curves are calculated from the engineering stress–strain curves by assuming a uniform deformation.

2.4. Transmission electron microscopy (TEM)

The TEM was performed using an FEI Tecnai F30 microscope operating at 300 kV. Specimens for TEM were taken from a location corresponding to the gauge section of the tensile specimen. They were prepared by mechanical grinding to a thickness of about 10 μm and then further thinning to a thickness of electron transparency using a Gatan Dual Ion Milling System with an Ar^+ accelerating voltage of 4 kV and liquid nitrogen to cool the specimen.

3. Experimental results

3.1. Mechanical properties

Fig. 2 shows the tensile mechanical behavior of the UFG Cu, Cu–10 wt.% Zn, and Cu–30 wt.% Zn samples. As shown in Fig. 2a, the yield strength and the ultimate strength increase with decreasing stacking fault energy from Cu to Cu–10 wt.% Zn to Cu–30 wt.% Zn (increasing Zn content in the alloy). However, the uniform elongation and the total elongation to failure first increase with decreasing stacking fault energy and then decrease, such that the Cu–10 wt.% Zn alloy exhibits the highest ductility. These results demonstrate there is an optimum stacking fault energy that yields the highest ductility. For convenience, the mechanical properties of these samples are listed in Table 1.

Fig. 2b shows the normalized strain hardening rate against the true plastic strain or the true stress (insert). It is obvious that the Cu–10 wt.% Zn alloy sample has a higher strain hardening rate than the UFG Cu sample at true plastic strains large than 2.5% and this provides an explanation for the higher ductility. The UFG Cu–30 wt.% Zn alloy sample has the highest normalized strain hardening rate when the true plastic strain is smaller than 2.5% but its ductility is the lowest. When the true plastic strain is larger than 2.5%, the strain hardening rate of the Cu–30 wt.% Zn alloy sample decreases below that of the Cu–10 wt.% Zn alloy sample. The strain hardening rate behavior of the Cu–30 wt.%

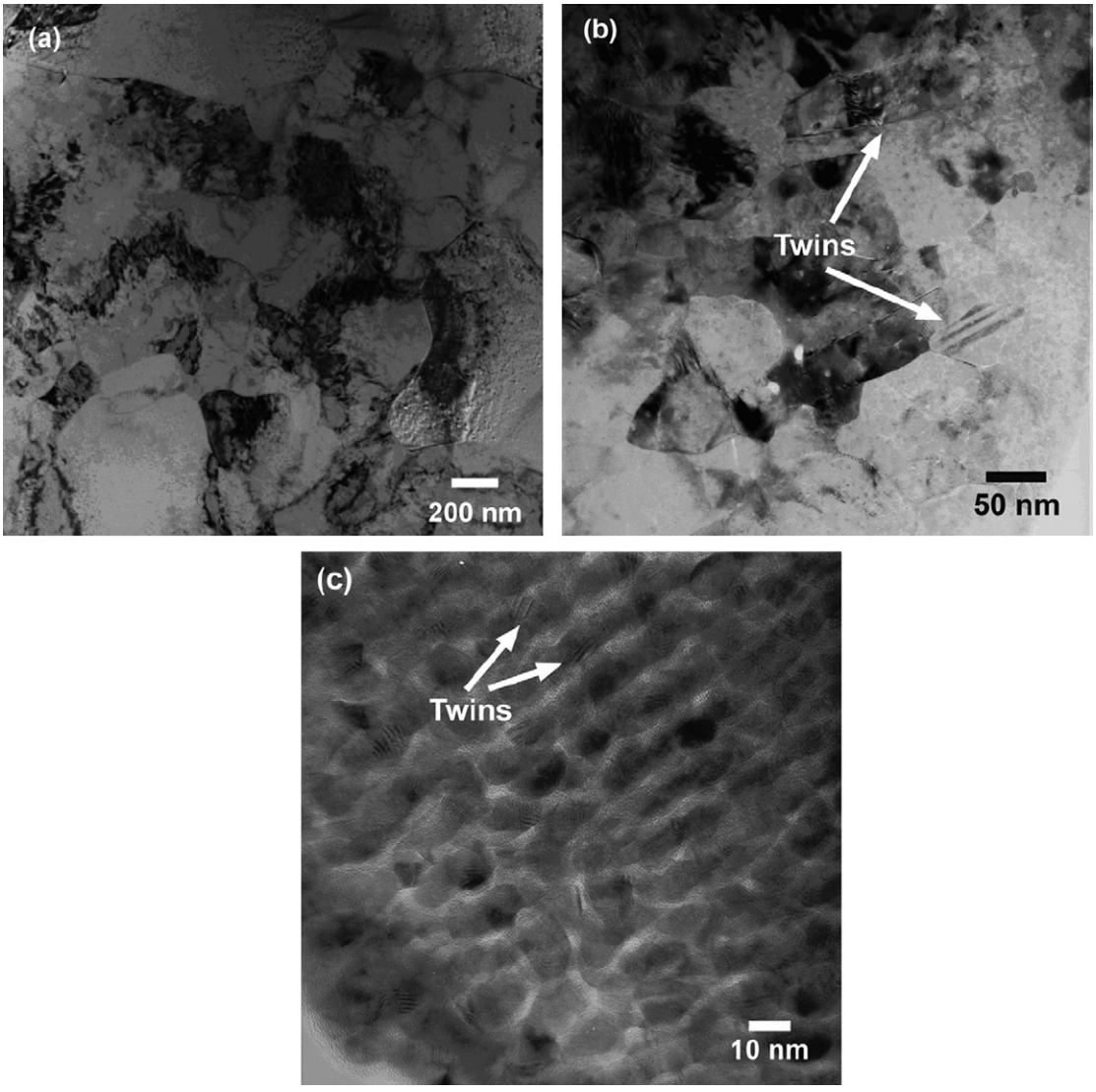

Fig. 3. Typical bright-field TEM images from the gauge sections of tensile samples (HPT + cold-rolling) of (a) the UFG Cu, (b) Cu–10 wt.% Zn sample [22] and (c) Cu–30 wt.% Zn before tensile tests.

Zn alloy sample is due to its unique microstructure which is shown and discussed in the following sections.

3.2. Microstructures and defects

Fig. 3 shows typical bright-field TEM images of the UFG Cu, Cu–10 wt.% Zn [22], and Cu–30 wt.% Zn samples before tensile testing. These TEM samples were taken from locations that correspond to the gauge sections of the tensile samples. As shown, the grain sizes decrease dramatically with decreasing stacking fault energy from the Cu sample (Fig. 3a) to the Cu–10 wt.% Zn sample (Fig. 3b) to the Cu–30 wt.% Zn sample (Fig. 3c). In addition, twins were observed in the Cu–10 wt.% Zn and Cu–30 wt.% Zn samples but not in the Cu sample. Moreover, the grains are irregular shape (Fig. 3a and b) or elongated shape (Fig. 3b and c). The sharp and straight boundaries in Fig. 3b are twin boundaries. XRD measurement indicates that rolling produced a (2 2 0) texture, the intensity of which decreases with decreasing stacking fault energy.

The statistical grain size distributions from TEM images of the three samples are shown in Fig. 4, where these distributions were achieved after processing by HPT + cold-rolling and they correspond to the gauge sections of the tensile samples. A total of 300 grains was measured for each distribution. For the Cu–30 wt.% Zn alloy sample, the measured grain size was the grain width. It can be seen in Fig. 4 that the average grain size decreases from 180 nm to 10 nm with decreasing SFE. Furthermore, these grain sizes are larger than those occurring in samples processed by HPT alone as documented in an earlier report [23]. This is due to the general non-uniformity of the HPT-processed samples [20–23]. Thus, the TEM images in Fig. 3 were taken from samples at locations corresponding to the gauge sections of the tensile samples and these grain sizes are larger than those near the edges of the disk reported previously [23]. In addition, there is also a possibility of grain growth during the cold rolling [24]. Fig. 4 also shows that the width of the grain size distribution is reduced with decreasing stacking fault energy, thereby demonstrating that the grain structure becomes more uniform as the stacking fault energy is reduced.

Fig. 5 shows high-resolution TEM images of (a) deformation twins and (b) stacking faults in the UFG Cu–10 wt.% Zn sample [16]. The stacking faults in Fig. 5b are especially interesting because they have limited width and lie inside a grain, thereby suggesting they were formed by dissociation of full dislocations. It is important to note also that such staking faults were not observed in the nanocrystalline Cu processed by HPT [25,26] but were observed in nanocrystalline Al [27,28]. It is not clear why the Cu–10 wt.% Zn alloy behaves differently from Cu and this is an issue that warrants further investigation. However, it is possible that the high density of stacking faults may interact effectively with slipping dislocations to increase the strain hardening rate.

A high-resolution TEM image of the high density of deformation twins in the UFG Cu–30 wt.% Zn sample is shown in Fig. 6 where the insert is the enlarged image of a threefold twin. Such multifold twins usually appear in nanocrystalline

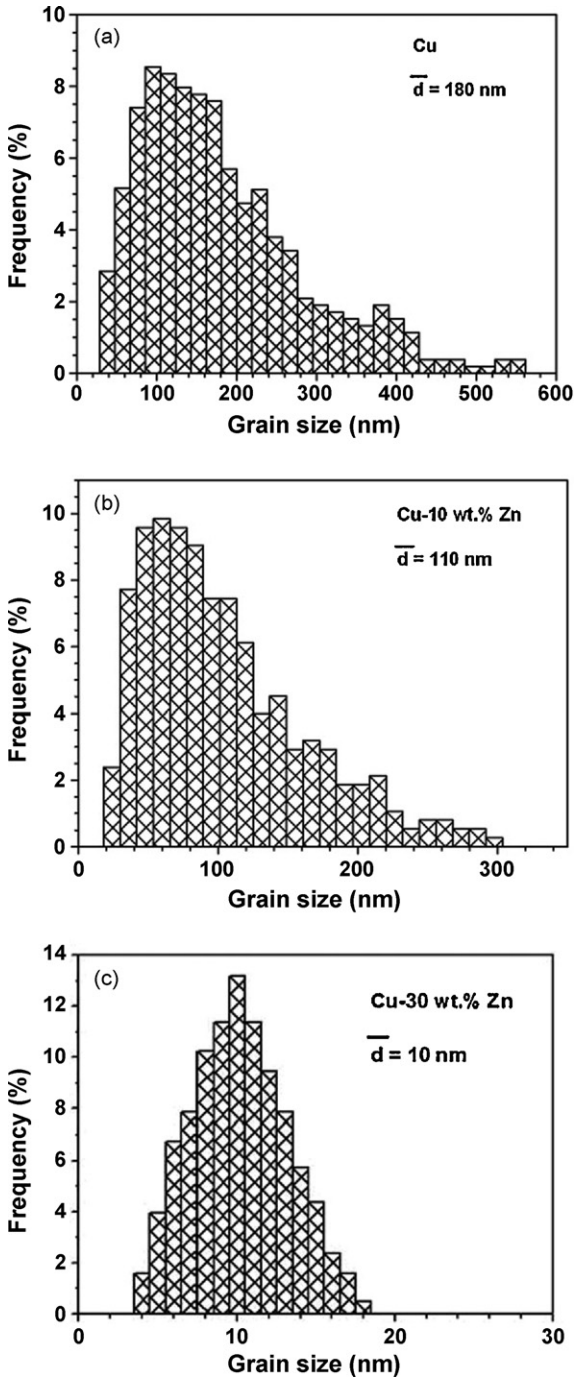

Fig. 4. Grain size distributions after HPT + cold-rolling in (a) Cu [22], (b) Cu–10% Zn sample [22] and (c) Cu–10 wt.% Zn sample before tensile tests.

fcc metals with small grain sizes [25,29–31] and are formed by a sequential twinning mechanism [31,32].

Table 2 lists the crystallite sizes, dislocation densities, twin densities and lattice parameters measured using XRD analysis. The twin density, β, is defined as the probability of finding a twin boundary between any two neighboring {1 1 1} planes [17]. As shown, the crystalline sizes for the Cu and UFG Cu–10 wt.% Zn samples are smaller than the grain sizes measured from the TEM micrographs. This difference is anticipated because the X-rays measure coherent diffraction domains [33,34] which include

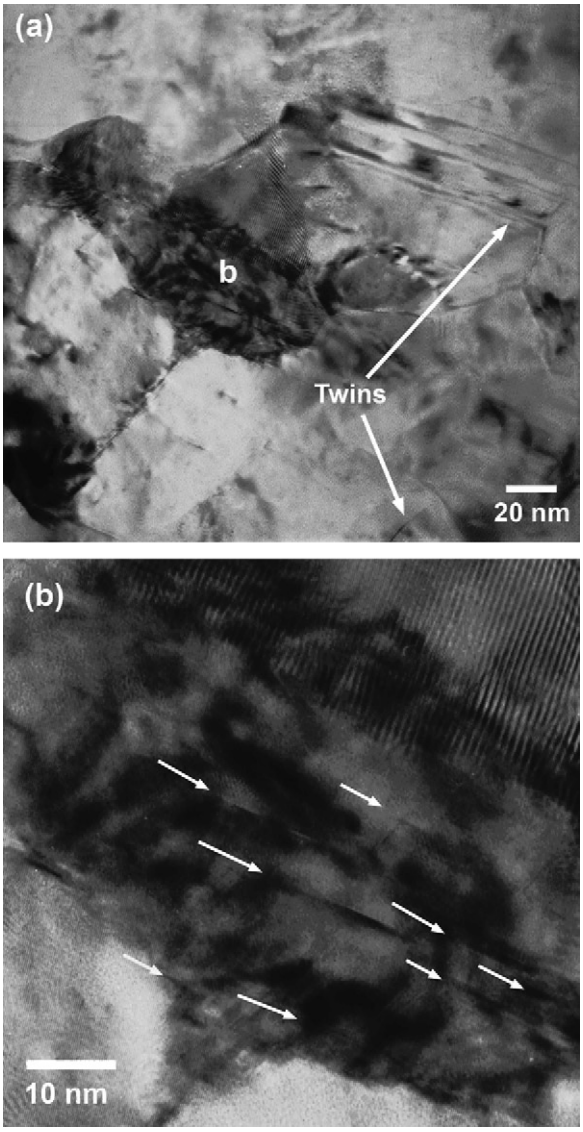

Fig. 5. High-resolution TEM images to show both deformation twins (a) and stacking faults (b) in the UFG Cu–10 wt.%Zn sample [16].

Table 2
Lists of the XRD-measured average grain sizes (d), dislocation density (ρ), twin density (β), and lattice parameters (a) of the HPT + cold-rolling processed Cu, Cu–10 wt.% Zn sample and Cu–30 wt.% Zn sample in the as-processed state (before tensile testing)

	Samples		
	Cu (99.9%)	Cu–10 wt.% Zn	Cu–30 wt.% Zn
d (nm)			
d_{XRD}	70	50	15
d_{TEM}	180	110	10
ρ ($\times 10^{15}$ m^{-2})	0.23	0.59	3.10
β (%)	0.1	4.8	8.0
a (nm)	0.3617	0.3640	0.3690

The errors of the XRD-measured grain sizes and dislocation density are less than 20%. The errors of the lattice parameters are ~0.0005 nm.

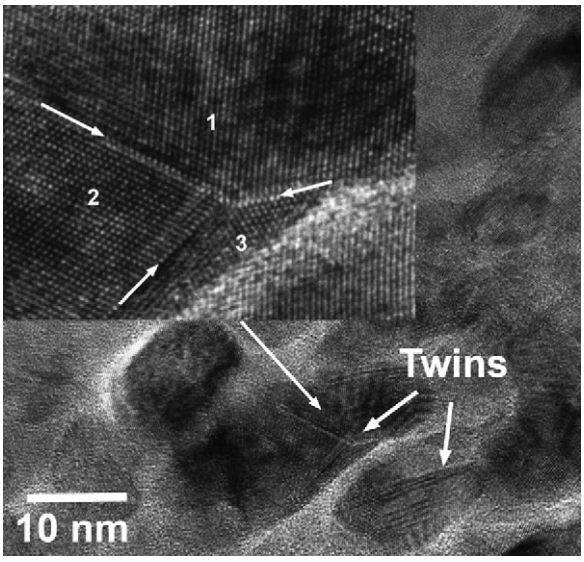

Fig. 6. High-resolution TEM images to show deformation twins in the UFG Cu–30 wt.% Zn. Insert shows a threefold twins.

dislocation cells and subgrains. By contrast, the crystallite size measured for the UFG Cu–30 wt.% Zn sample is larger than the grain size from the TEM micrograph. This may be caused by an overlapping of small grains in the TEM micrographs which would lead to an apparently smaller grain size. Thus, it is suggested that the grain size measured from TEM micrograph may underestimate the true grain size if the grain size is too small [24]. Table 2 also shows that both the dislocation density and twin density increase dramatically with decreasing stacking fault energy from the Cu sample to the UFG Cu–10 wt.% Zn sample to the UFG Cu–30 wt.% Zn sample. As discussed in the following section, these observations have a significant impact on the ductility.

4. Discussion

Fig. 2a clearly shows that the UFG Cu–10 wt.% Zn sample, which has a stacking fault energy higher than that of the Cu–30 wt.% Zn sample but lower than that of the Cu, has the highest uniform elongation and total elongation. To investigate the reasons for the variation in the strain hardening rates of the three samples, the dislocation density and twin density were measured after the tensile testing of the samples using X-ray analysis.

The results are summarized in Table 3 where it is apparent that the dislocation density in UFG Cu increases only by 0.5×10^{14} m^{-2} during the tensile testing, giving the lower strain hardening rate and uniform elongation shown in Fig. 2. The twin density does not change indicating that deformation twinning was not activated. In contrast, the UFG Cu–10 wt.% Zn sample experiences both dislocation accumulation (by 1.4×10^{14} m^{-2}) and twin accumulation (by 0.7%), thereby explaining its relatively higher strain hardening rate and high uniform elongation. It is surprising that the Cu–30 wt.% Zn sample shows no change either in the dislocation density or in the twin density before and after the tensile tests although this alloy has the high-

Table 3
Change of dislocation density, ρ, and twin density, β, before and after tensile testing of the UFG Cu, Cu–10 wt.% Zn, and Cu–30 wt.% Zn samples

	Samples		
	Cu (99.9%)	Cu–10 wt.% Zn	Cu–30 wt.% Zn
ρ ($\times 10^{14}$ m^{-2}) before	2.3	5.9	31.0
ρ ($\times 10^{14}$ m^{-2}) after	2.8	7.3	31.0
Change in ρ ($\times 10^{14}$ m^{-2})	0.5	1.4	0
β (%) before	0.1	4.8	8.0
β (%) after	0.1	5.5	8.0
Change in β (%)	0	0.7	0

est strain hardening at true plastic strains smaller than 2.5%. Therefore, it is concluded that its strain hardening during the tensile testing was not caused by either dislocation or twin accumulations.

The lack of change in defect density in the Cu–30 wt.% Zn before and after the tensile tests can be understood from its grain and defect structures in the as-processed state. First, the grain size of this sample is exceptionally small (~15 nm) so that dislocations are easily annihilated at grain boundaries without accumulations [1,34]. Second, as listed in Table 3, the dislocation and twin densities are already very high before the tensile testing and it is probable they are already in saturated states. If this interpretation is correct, it would be impossible to further accumulate dislocations or twins. Therefore, it is reasonable to speculate that the ductility of the Cu–30 wt.% Zn sample may be increased by annealing to reduce the dislocation and twin densities.

The very high strain hardening rate observed in the Cu–30 wt.% Zn may be caused by grain rotation and grain boundary sliding due to the extremely small grain size. Such mechanisms have been reported in UFG/nanostructured materials with comparable or much larger grain sizes [25,35–37]. It is not clear how grain rotation and/or grain boundary sliding will affect the ductility. Nevertheless, since the dislocation and twin density remain unchanged before and after the tensile testing, the strain hardening observed in Fig. 2 for the Cu–30 wt.%Zn alloy may arise from the occurrence of grain rotation/grain boundary sliding. Similar mechanical behavior was also reported recently in nanocrystalline Ni and its alloys and it was attributed to the grain size distribution and the reduction of elastic grains with increasing stress [38,39]. The mechanism responsible for the initially high strain hardening rate is an interesting and fundamental issue that requires further investigation.

5. Conclusions

It is shown that there exists an optimal stacking fault energy yielding the best ductility in UFG metals and alloys with the same deformation processing strain. The small grain size of the UFG CuZn alloy with low stacking fault energy is the main reason for its low ductility. The key to improving the ductility is to improve the strain hardening rate via dislocation accumulation and twin accumulation. Annealing may be able to improve the ductility by reducing the dislocation and twin density in UFG metals and alloys processed by SPD techniques, especially for those with very low stacking fault energies. The observed effect of stacking fault energy on the ductility should be taken into consideration in designing UFG and nanostructured alloys for high strength and high ductility.

References

[1] D. Jia, Y.M. Wang, K.T. Ramesh, E. Ma, Y.T. Zhu, R.Z. Valiev, Appl. Phys. Lett. 79 (2001) 611.
[2] R.Z. Valiev, I.V. Alexandrov, Y.T. Zhu, T.C. Lowe, J. Mater. Res. 17 (2002) 5.
[3] Y. Wang, M. Chen, F. Zhou, E. Ma, Nature 419 (2002) 912.
[4] C.C. Koch, Scripta Mater. 49 (2003) 657.
[5] Y.T. Zhu, X.Z. Liao, Nat. Mater. 3 (2004) 351.
[6] K.M. Youssef, R.O. Scattergood, K.L. Murty, J.A. Horton, C.C. Koch, Appl. Phys. Lett. 87 (2005) 091904.
[7] R.Z. Valiev, Y. Estrin, Z. Horita, T.G. Langdon, M.J. Zehetbauer, Y.T. Zhu, JOM 58 (4) (2006) 33.
[8] L. Lu, Y. Shen, X. Chen, L. Qian, K. Lu, Science 304 (2004) 422.
[9] E. Ma, Y.M. Wang, Q.H. Lu, M.L. Sui, L. Lu, K. Lu, Appl. Phys. Lett. 85 (2004) 4932.
[10] Y.B. Lee, D.H. Shin, K.T. Park, W.J. Nam, Scripta Mater. 51 (2004) 355.
[11] H.W. Höppel, J. May, M. Göken, Adv. Eng. Mater. 6 (2004) 781.
[12] B.Q. Han, Z. Lee, D. Witkin, S. Nutt, E.J. Lavernia, Metall. Mater. Trans. A 36 (2005) 957.
[13] Z. Horita, K. Ohashi, T. Fujita, K. Kaneko, T.G. Langdon, Adv. Mater. 17 (2005) 1599.
[14] H.W. Kim, S.B. Kang, N. Tsuji, Y. Minamino, Acta Mater. 53 (2005) 1737.
[15] Y.H. Zhao, X.Z. Liao, S. Cheng, E. Ma, Y.T. Zhu, Adv. Mater. 18 (2006) 2280.
[16] Y.H. Zhao, Y.T. Zhu, X.Z. Liao, Z. Horita, T.G. Langdon, Appl. Phys. Lett. 89 (2006) 121906.
[17] Y.H. Zhao, J.F. Bingert, X.Z. Liao, B.Z. Cui, K. Han, A.V. Sergueeva, A.K. Mukherjee, R.Z. Valiev, T.G. Langdon, Y.T. Zhu, Adv. Mater. 18 (2006) 2949.
[18] K.X. Tao, H. Choo, H.Q. Li, B. Clausen, J.E. Jin, Y.K. Lee, Appl. Phys. Lett. 90 (2007) 101911.
[19] C.B. Carter, I.L.F. Ray, Philos. Mag. 35 (1977) 189.
[20] H.G. Jiang, Y.T. Zhu, D.P. Butt, I.V. Alexandrov, T.C. Lowe, Mater. Sci. Eng. A 290 (2000) 128.
[21] A.P. Zhilyaev, G.V. Nurislamova, B.-K. Kim, M.D. Baró, J.A. Szpunar, T.G. Langdon, Acta Mater. 51 (2003) 753.
[22] Y.H. Zhao, X.Z. Liao, Y.T. Zhu, Z. Horita, T.G. Langdon, Mater. Sci. Eng. A 463 (2007) 22.
[23] Y.H. Zhao, X.Z. Liao, Y.T. Zhu, Z. Horita, T.G. Langdon, Mater. Sci. Eng. A 410–411 (2005) 188.
[24] X.Z. Liao, R.Z. Valiev, H.S. Gao, X.D. Li, A.K. Mukherjee, J.F. Bingert, Y.T. Zhu, Appl. Phys. Lett. 88 (2006) 021909.
[25] X.Z. Liao, Y.H. Zhao, S.G. Srinivasan, Y.T. Zhu, R.Z. Valiev, D.V. Gunderov, Appl. Phys. Lett. 84 (2004) 592.
[26] X.Z. Liao, Y.H. Zhao, Y.T. Zhu, R.Z. Valiev, D.V. Gunderov, J. Appl. Phys. 96 (2004) 636.
[27] X.Z. Liao, F. Zhou, E.J. Lavernia, S.G. Srinivasan, M.I. Baskes, D.W. He, Y.T. Zhu, Appl. Phys. Lett. 83 (2003) 632.
[28] X.Z. Liao, S.G. Srinivasan, Y.H. Zhao, M.I. Baskes, Y.T. Zhu, F. Zhou, E.J. Lavernia, H. Xu, Appl. Phys. Lett. 84 (2004) 3564.
[29] J.Y. Huang, Y.K. Wu, H.Q. Ye, Acta Mater. 44 (1996) 1121.
[30] X.Z. Liao, J.Y. Huang, Y.T. Zhu, F. Zhou, E.J. Lavernia, Philos. Mag. 83 (2003) 3065.
[31] Y.T. Zhu, X.Z. Liao, R.Z. Valiev, Appl. Phys. Lett. 86 (2005) 103112.
[32] A.J. Cao, Y.G. Wei, Appl. Phys. Lett. 89 (2006) 041919.

[33] T. Ungár, L. Balogh, Y.T. Zhu, Z. Horita, C. Xu, T.G. Langdon, Mater. Sci. Eng. A 444 (2007) 153.
[34] Y.T. Zhu, J.Y. Huang, J. Gubicza, T. Ungár, Y.M. Wang, E. Ma, R.Z. Valiev, J. Mater. Res. 18 (2003) 1908.
[35] Z. Shan, E.A. Stach, J.M.K. Wiezorek, J.A. Knapp, D.M. Follstaedt, S.X. Mao, Science 305 (2004) 654.
[36] N.Q. Chinh, P. Szommer, Z. Horita, T.G. Langdon, Adv. Mater. 18 (2006) 34.
[37] N.Q. Chinh, P. Szommer, T. Csanádi, T.G. Langdon, Mater. Sci. Eng. A 434 (2006) 326.
[38] H. Li, F. Ebrahimi, Appl. Phys. Lett. 84 (2004) 4307.
[39] F. Ebrahimi, Z. Ahmed, H. Li, Appl. Phys. Lett. 85 (2004) 3749.